



OPEN

Tracing the subducting Pacific slab to the mantle transition zone with hydrogen isotopes

Takeshi Kuritani^{1✉}, Kenji Shimizu², Takayuki Ushikubo², Qun-Ke Xia³, Jia Liu³, Mitsuhiro Nakagawa¹, Hajime Taniuchi⁴, Eiichi Sato⁵ & Nobuo Doi⁶

Hydrogen isotopes have been widely used as powerful tracers to understand the origin of terrestrial water and the water circulation between the surface and the deep interior of the Earth. However, further quantitative understanding is hindered due to a lack of observations about the changes in D/H ratios of a slab during subduction. Here, we report hydrogen isotope data of olivine-hosted melt inclusions from active volcanoes with variable depths (90–550 km) to the subducting Pacific slab. The results show that the D/H ratio of the slab fluid at the volcanic front is lower than that of the slab fluid just behind the volcanic front. This demonstrates that fluids with different D/H ratios were released from the crust and the underlying peridotite portions of the slab around the volcanic front. The results also show that the D/H ratios of slab fluids do not change significantly with slab depths from 300 to 550 km, which demonstrates that slab dehydration did not occur significantly beyond the arc. Our estimated $\delta D\text{‰}$ value for the slab materials that accumulated in the mantle transition zone is $> -90\text{‰}$, a value which is significantly higher than previous estimates.

Global water cycles involving the Earth's deep interior have played a critical role in Earth's evolution^{1–5}. Water in the Earth's mantle affects its rheological and melting behaviours, thereby controlling the thermal evolution and chemical differentiation of the solid Earth². The ocean's mass is primarily controlled by the balance between the water influx to the interior through subducting oceanic plates and the water outflux to the surface through magmatism^{3–5}. Understanding the origin of terrestrial water and the cycling and distribution of water in the Earth's interior has been significantly improved by the application of stable hydrogen isotopes, which are powerful tracers^{6–13}. As materials transported into the Earth's interior by subduction decrease the hydrogen isotope (D/H) ratios by releasing Deuterium (D)-enriched fluids⁹, D/H ratios of deep-source magmas allow us to identify the involvement of the recycled water as well as distinguish the recycled water from the Earth's primordial water.

Little is understood about the changes in the D/H ratio of subducting slabs with increasing depth, which is a key issue in estimating the characteristic D/H ratios of subducted recycled materials in the deep mantle reservoir. Using the results of hydrogen isotopic analyses on olivine-hosted melt inclusions for some Mariana arc volcanoes, Shaw et al.⁹ estimated the $\delta D\text{‰}$ values ($\delta D\text{‰} = [(D/H)_{\text{sample}} - (D/H)_{\text{SMOW}}]/(D/H)_{\text{SMOW}} \times 1000$, where SMOW refers to the standard mean ocean water, and $\delta D = 0\text{‰}$) of the subducted materials after 92% dehydration¹⁴ to be as low as -234‰ . Walowski et al.¹¹ estimated the $\delta D\text{‰}$ values of dehydrated residual slab materials to be -100‰ to -120‰ by combining the results of hydrogen isotopic analyses on melt inclusions from Cascadia arc basalts with a model that considered the thermal and petrological structures of a hot subducting slab. So far, however, the evolution of the D/H ratios of the subducting materials beyond the frontal arc has not been well defined by natural observations. This is partly because the density of volcanoes decreases from the volcanic front to the rear-arc side, and the number of rear-arc volcanoes is relatively small (subduction zone volcanoes with slab depths (Z) of > 150 km are only $\sim 7\%$)¹⁵. In addition, subduction zone magmas typically contain appreciable amounts of volatiles, and, resultingly, they commonly degas during their ascent to the surface. Therefore, to estimate the D/H ratios of magma at depths using subaerial volcanic products, it is necessary to analyse melt inclusions (typically < 100 μm in diameter) trapped in phenocrysts^{9,11}. However, it is challenging to obtain high-quality

¹Department of Earth and Planetary Sciences, Faculty of Science, Hokkaido University, Sapporo, Japan. ²Kochi Institute for Core Sample Research, Japan Agency for Marine-Earth Science and Technology, Nankoku, Japan. ³Key Laboratory of Geoscience Big Data and Deep Resource of Zhejiang Province, School of Earth Sciences, Zhejiang University, Hangzhou, China. ⁴Department of Natural History Sciences, Graduate School of Science, Hokkaido University, Sapporo, Japan. ⁵Earth Science Laboratory, Hokkaido University of Education, Asahikawa, Japan. ⁶Research Center for Regional Disaster Management, Iwate University, Morioka, Japan. ✉email: kuritani@sci.hokudai.ac.jp

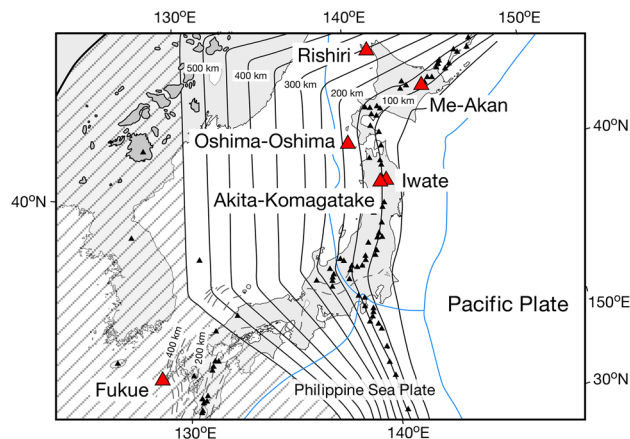


Figure 1. Map showing the distribution of active volcanoes above the subducted Pacific slab. The studied active volcanoes are shown here: Iwate ($Z \sim 90$ km), Akita-Komagatake ($Z \sim 100$ km), Me-Akan ($Z \sim 110$ km), Oshima-Oshima ($Z \sim 180$ km), Rishiri ($Z \sim 300$ km), and Fukue ($Z \sim 550$ km). The slab depths were sourced from Refs.^{38,39}. The grey patches denote representative Cenozoic volcanic fields in China⁴⁰. The solid and dashed contour lines denote the depths of the upper boundaries of the subducting Pacific and Philippine Sea slabs, respectively³⁹. The blue lines denote the plate boundaries at the surface. The shaded area indicates the range of the stagnant Pacific slab at depths $> \sim 550$ km in the MTZ⁴¹. This figure was created using Canvas 14.

hydrogen isotopic data on samples of such small sizes. Furthermore, D/H data of the melt inclusions should be used carefully, because the ratios do not necessarily represent those of the original magma due to degassing and post-entrapment modification of the melt inclusion compositions by shallow-level processes^{9,11,16,17}.

In this study, to trace the evolution of the D/H ratios of the subducting Pacific slab from the volcanic front to the mantle transition zone (MTZ), the hydrogen isotopic compositions of olivine-hosted melt inclusions were determined for basaltic scoria samples from six active volcanoes, including Iwate ($Z \sim 90$ km), Akita-Komagatake ($Z \sim 100$ km), Me-Akan ($Z \sim 110$ km), Oshima-Oshima ($Z \sim 180$ km), Rishiri ($Z \sim 300$ km), and Fukue ($Z \sim 550$ km) (Fig. 1). The Iwate, Akita-Komagatake, and Oshima-Oshima volcanoes belong to the NE Japan arc, and the Me-Akan and Rishiri volcanoes belong to the Kuril arc. Fukue is an intraplate-type volcano, beneath which the subducted Pacific Plate is stagnated in the MTZ (Fig. 1). The MTZ here is considerably hydrous, as shown by electrical conductivity observations¹⁸. The influx of fluids derived from the stagnant Pacific slab generates primary magmas from the melting of the asthenospheric mantle at the Fukue volcano¹⁹. Therefore, the samples from the five arc volcanoes and the Fukue volcano provide information about the variations in the D/H ratios of fluids released from the cold subducting Pacific slab at depths from ~ 90 to ~ 550 km. Notably, the slab depth of ~ 300 km for Rishiri is one of the deepest among arc volcanoes globally, and Fukue is one of the rare active volcanoes that originated from the magmatism rooted in the MTZ.

Numerous scoria samples were collected from various tephra fall deposits at different eruption stages for each of the six volcanoes, and the deposits containing scoria with the highest-quality olivine-hosted melt inclusions were carefully selected. The melt inclusion-bearing olivine crystals were then separated from the scoria samples collected from the selected deposits. To carefully examine the effect of the post-entrapment modification of melt inclusions, volatile content analyses were conducted on at least 25 melt inclusions for each volcano (37 for Iwate, 30 for Akita-Komagatake, 25 for Me-Akan, 38 for Oshima-Oshima, 48 for Rishiri, and 43 for Fukue). Hydrogen isotopic analyses were conducted primarily on melt inclusions with higher H_2O contents for each volcano. Some melt inclusions with lower H_2O contents were also measured to assess the variations in the D/H ratio with varied H_2O content.

Results and discussion

The descriptions of the scoria samples used in this study are provided in Supplementary Methods. The samples exhibit basaltic compositions (Supplementary Table S1) and contain olivine as the primary mafic phenocryst phase. The samples from the Iwate, Akita-Komagatake, Me-Akan, Oshima-Oshima, and Rishiri volcanoes show trace element concentration patterns that are characteristic of arc basalt. In contrast, the trace element concentration pattern for the samples from the Fukue volcano has an affinity to intra-plate basalt (Supplementary Fig. S1). The Pb isotopic compositions of all the samples lie within the triangular field defined by three subduction zone components: sediment, altered oceanic crust, and depleted mantle (Supplementary Fig. S2).

Volatile (H_2O , CO_2 , F, S, and Cl) and P_2O_5 contents and hydrogen isotopic compositions were analysed on melt inclusions using the ion microprobe (Cameca IMS-1280HR, Ametek Cameca) at the Kochi Institute for Core Sample Research, JAMSTEC. As most measured melt inclusions were glassy without daughter minerals (Supplementary Fig. S3), we did not homogenise the inclusions at high temperatures. The details of the analytical procedures, including sample preparation, analytical conditions, and standard data, are provided in Refs.^{20,21} and “Methods”. The volatile and major elemental compositions and the $\delta D\%$ values of the melt inclusions are listed in Supplementary Table S2.

It is well established that the D/H ratios of olivine-hosted melt inclusions do not necessarily represent those of mantle-derived magmas^{9,11,16,17}. Mantle-derived magma is not saturated with volatiles at deep levels because volatiles are more soluble in melt at higher pressures. During the ascent of the magma in the crust, the magma becomes saturated with volatiles and vesiculation occurs. Degassing of the magma can cause fractionation of the D/H ratio²² because the D/H ratio of an H₂O-rich vapor phase is higher than that of the melt phase. In addition, during residence of the magma in a crustal magma chamber, the D/H ratio of the magma may be modified by crustal assimilation. Because of these, the D/H ratios of the melt inclusions entrapped in olivine phenocrysts after magma degassing and/or crustal assimilation can be significantly different from those of the original magma. As the magma continues to further ascend, the H₂O content of the melt progressively decreases. The D/H ratios of olivine-hosted melt inclusions that were entrapped before the magma degassing can be modified by the re-equilibration of the olivine with the surrounding melt because of faster diffusion of H relative to D through the host olivine^{16,17}. For these reasons, to extract the information about the mantle processes from melt inclusion data, it is necessary to carefully evaluate the effects of shallow-level processes on the D/H ratios.

The volatile content data are shown in CO₂–H₂O diagrams for all the melt inclusions from the individual volcanoes in Supplementary Figs. S4–S9. At all the volcanoes, the melt inclusions have variable H₂O contents, and those with relatively higher H₂O contents have highly variable CO₂ contents at a given H₂O content. Some melt inclusions have shrinkage bubbles, and, therefore, the original CO₂ contents would have been even higher¹⁷. CO₂ is the first compound to be lost by degassing during magma ascent from the upper mantle because it is the least soluble species in silicate melt among the major volatile elements²³. Therefore, the marked variation in CO₂ content at a given H₂O content suggests that the melt with high CO₂ and high H₂O contents experienced minimal loss of H₂O by degassing before the entrapment²⁴. In contrast, the low CO₂ and low H₂O contents of some melt inclusions may be explained by the entrapment of melts that were degassed during magma ascent (i.e. open-system and closed-system degassing trends in Supplementary Fig. S6a). The high CO₂ melt inclusions trapped at high pressures might have experienced re-equilibration with lower H₂O melt through the host olivine at lower pressures, as explained above. $\delta D\%$ values of the melt inclusions are expected to correlate negatively with the H₂O contents when a diffusive loss of H₂O occurs significantly from the melt inclusions^{16,17}. At all the volcanoes, some melt inclusions with lower H₂O contents tend to have higher $\delta D\%$ values, and they might have been affected by diffusive re-equilibration. However, the $\delta D\%$ values and the H₂O content of CO₂-rich melt inclusions do not exhibit a significant negative correlation, suggesting that CO₂-rich melt inclusions did not experience significant diffusive re-equilibration. This is consistent with the observation that the $\delta D\%$ values of the high CO₂ melt inclusions are essentially constant irrespective of the CO₂ contents (Supplementary Figs. S4–S9). Based on these evaluations, the data of the melt inclusions with the three highest CO₂ contents were selected as the representative data sets for each volcano.

Of the remaining melt inclusions, some inclusions with high H₂O and lower CO₂ contents may also preserve the original D/H ratios, because they experienced minimal loss of H₂O by degassing from the original magma with high CO₂ and high H₂O contents (see the degassing trends in Supplementary Fig. S6a). However, these inclusions were entrapped at lower pressures than those with high CO₂ contents, and there would be a possibility that the magmas experienced additional processes such as crustal assimilation before the entrapment at the shallow levels. Therefore, the data of the inclusions with low CO₂ contents were not used as the representative data sets for each volcano.

The average H₂O contents of the three representative inclusions are 3.5 wt.% for Iwate, 2.7 wt.% for Akita-Komagatake, 3.8 wt.% for Me-Akan, 4.1 wt.% for Oshima-Oshima, 3.8 wt.% for Rishiri, and 2.0 wt.% for Fukue. The Cl/F and H₂O/F ratios of the melt inclusions are shown as a function of the slab depth in Fig. 2a,b, respectively. These ratios are significantly higher for all the volcanoes than those of the depleted mantle or the majority of mid-ocean ridge basalts (MORB)^{25,26}. This observation reconfirms that the fluids derived from the Pacific slab were involved in the magma genesis for the volcanoes. In particular, the involvement of the slab-derived fluids at the Fukue volcano supports the 'Big mantle wedge model'^{27,28}, according to which deep dehydration from the stagnant slab in the MTZ plays a primary role in the overlying volcanism. Notably, the slab fluids for the Fukue volcano were not derived from the Philippine Sea Plate because the plate is too hot to efficiently carry water to the depths of the MTZ¹⁹. The Cl/F and H₂O/F ratios at Fukue ($Z = \sim 550$ km) are lower than those of the frontal-arc Iwate and Me-Akan volcanoes. This can be attributed to preferential partitioning of Cl and H₂O into slab fluids relative to F over the slab source materials²⁹.

The $\delta D\%$ values of the representative melt inclusions are plotted against the slab depths in Fig. 2c. The value of $-80 \pm 10\%$ ⁷ was commonly used as the reference $\delta D\%$ value for the depleted mantle, and it was later revised to $-60 \pm 5\%$ ³⁰. However, recent work suggests that the $\delta D\%$ values of the depleted mantle could be heterogeneous worldwide, and this value for some depleted MORB, such as those from the North Atlantic, is $-90 \pm 10\%$ ¹². The present study used the traditional $\delta D\%$ value of $-80 \pm 10\%$ for the Pacific depleted mantle. The $\delta D\%$ values of the samples from all the volcanoes are higher than those of the depleted mantle, which can be interpreted to result from the addition of D-enriched slab fluids to the source depleted mantle⁹. The water dissolved in a subduction-related primary magma is derived from the H₂O in the slab-derived fluid and the H₂O contained in the depleted mantle peridotite. We estimated that the contributions of the slab fluids to the H₂O budget in the primary magmas from the studied volcanoes range from 92 to 98% (Supplementary Methods), and hence, the $\delta D\%$ values of the representative melt inclusions (Fig. 2c) can be regarded as those of the slab-derived fluids at the individual volcanoes.

One of the crucial observations is that the $\delta D\%$ values of Iwate are lower than those of Akita-Komagatake, which is located just behind the frontal arc of the Iwate volcano. This observation cannot be explained by the single reservoir model proposed in Ref.⁹. When the subducting slab behaves as a single H₂O reservoir, the D/H ratios of the slab fluids would decrease with increasing slab depth because of the continuous release of D-enriched fluids from the slab. Therefore, our observation requires the involvement of at least two H₂O reservoirs with

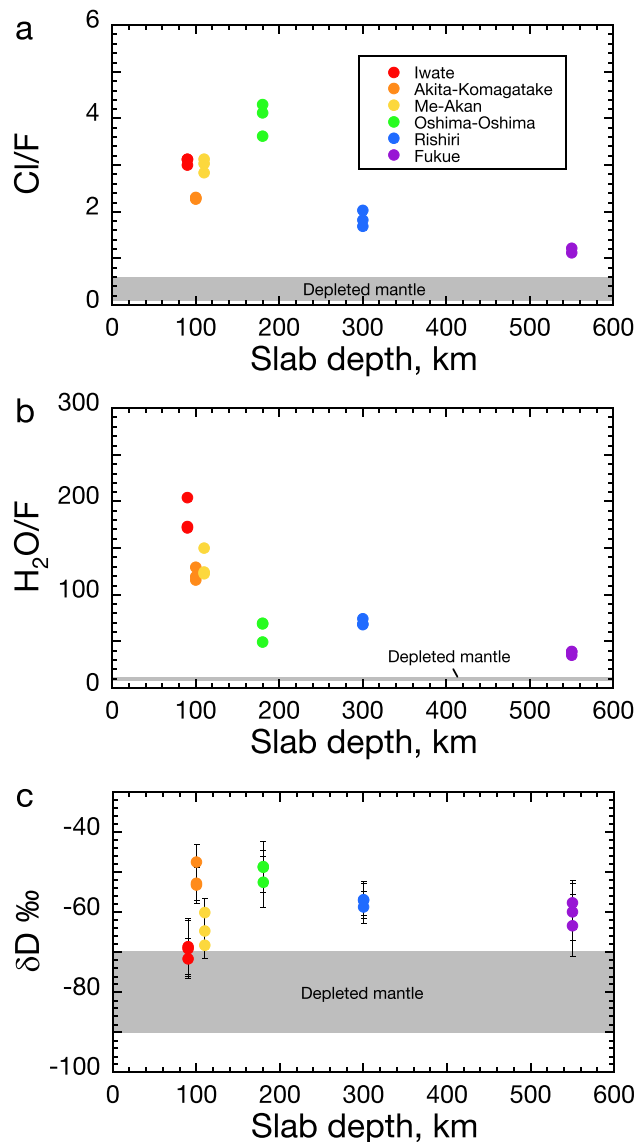


Figure 2. (a) Cl/F ratios, (b) H₂O/F ratios, and (c) δD‰ values of the representative olivine-hosted melt inclusions from the Iwate, Akita-Komagatake, Me-Akan, Oshima-Oshima, Rishiri, and Fukue volcanoes, plotted as a function of the depth of the subducting Pacific Plate. The values of the depleted mantle (or the majority of MORB) for the Cl/F ratios, H₂O/F ratios, and δD were sourced from Ref.²⁵, Ref.²⁶, and Ref.⁷, respectively.

different D/H ratios in the generation of slab fluids beneath the Iwate and nearby Akita-Komagatake volcanoes. Recently, the role of the slab peridotite layer as the H₂O source for subduction zone magmas has been receiving increased attention^{11,12,31}. The crust portion of the subducting slab, consisting of altered basaltic rocks [altered oceanic crust (AOC) and gabbro (GAB)] and sediment (SED), and the overlying mantle wedge base peridotite (MWP) are considerably dehydrated before reaching the depth beneath the volcanic front (Fig. 3). Contrastingly, the underlying peridotite portion of the slab (SlbP), which is effectively hydrated during bending at the trench, can survive as a water reservoir beneath the arc^{12,31} (Fig. 3). This scenario can explain the observed spatial variation in the δD‰ data. When the slab fluid for Iwate was supplied primarily from the crust portion of the slab (green star in Fig. 3), the D/H was likely low because this portion had already been considerably dehydrated at shallower levels. Conversely, the main source of the fluid beneath the Akita-Komagatake volcano is considered to have been the underlying peridotite portion of the slab (yellow star in Fig. 3). In this case, the fluid would be relatively D-enriched because this portion was not significantly dehydrated before reaching ~100 km depth. Therefore, considering that the initial D/H ratios of the crust and peridotite portions of the slab were similar at the time of the subduction, the fluid released at ~2.5 GPa from the crust portion would have lower D/H ratios than that released at ~3.5 GPa from the underlying peridotite portion^{11,12}. The low δD‰ values of the Me-Akan samples (–60 to –70‰) may also reflect that the slab fluid responsible for the magmatism was sourced primarily from the crust portion of the slab, considering that the volcano is located at the volcanic front of the Kuril arc.

The δD‰ values of the melt inclusions from the Mariana arc basalts are high, ranging from –55 to –12‰⁹, compared to those of the frontal-arc Iwate and Me-Akan volcanoes. This can be attributed to the fact that the

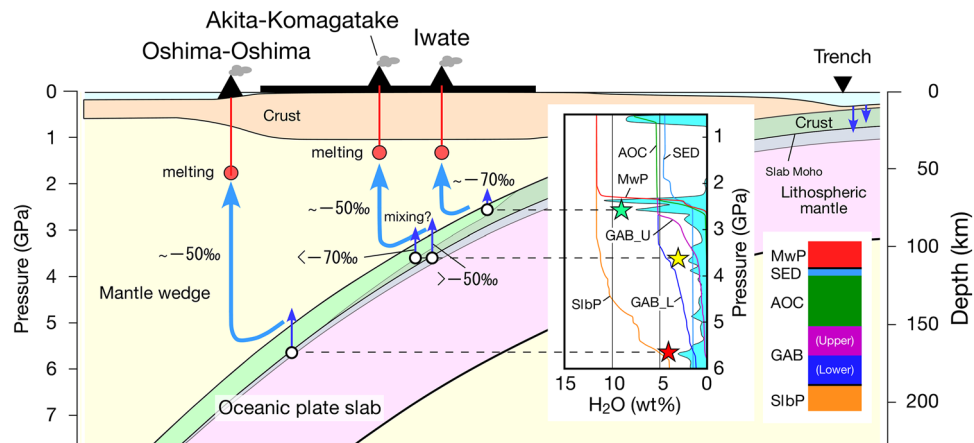


Figure 3. Schematic of the subduction-zone processes in the NE Japan arc. The figure is modified from Fig. 11A of Ref.⁴² illustrating the chemical geodynamics in a cold subduction system. The inset, modified from Fig. 2a of Ref.³¹, shows the result of calculations for the NE Japan arc using the Arc Basalt Simulator version 5. Namely, the results show variations in the total amount of H₂O released from the slab (the cyan area) and in the amounts of H₂O stored in the individual layers of the subducting slab with depth. MwP denotes the mantle wedge base peridotite layer just above the subducting slab; SED and AOC refer to the sediment layer and the altered oceanic crust layer, respectively; GAB_U and GAB_L denote the upper and lower gabbro layers, respectively; and SlbP refers to the slab peridotite layer. The green, yellow, and red stars indicate the possible main H₂O sources of the slab fluids for Iwate, Akita-Komagatake, and Oshima-Oshima, respectively. The red circles denote the melt segregation depths obtained by Refs.^{43,44} (the segregation depth at Oshima-Oshima is assumed to be similar to that at Sannome-gata⁴³). Fluids released from the slab surface may be dragged to a slightly deeper depth because they can be trapped in a triple junction of the olivine grains in the overlying mantle wedge base peridotite layer (MwP)³¹. This figure was created using Canvas 14.

low- δD fluid from the dehydrated crustal portion of the slab did not significantly contribute to the Mariana arc magmatism because of the deeper slab depths (~ 115 km)³² of the Mariana arc volcanoes. Alternatively, it is possible that the contribution of the low- δD fluid was obscured by the main high- δD fluid flux from the less-dehydrated peridotite portion of the slab because of the high dip angle (70° – 80°) of the Pacific slab in the Mariana arc compared with shallower angles (30° – 40°) in the NE Japan and Kuril arcs³³.

The δD ‰ values of Rishiri ($Z \sim 300$ km) are similar to those of Fukue ($Z \sim 550$ km). At levels deeper than ~ 150 km, the peridotite (SlbP) and gabbro (GAB_L) portions of the slab would be the main H₂O source^{31,34}, and water is supplied primarily by the breakdown of serpentine in the peridotite layer¹². No significant decrease in the δD ‰ values of slab fluids deeper than ~ 300 km suggests that significant dehydration of the peridotite portion of the slab did not occur during the subduction to the MTZ. This result is consistent with the observation that only a few instances of magmatism, including those of Rishiri and Fukue, are caused by a fluid release from the Pacific slab with $Z > \sim 200$ km. The host basalts of these samples (i.e. Rishiri and Fukue) have significantly enriched Pb isotopic features compared with the depleted mantle (Supplementary Fig. S2). This suggests that the fluids that were dehydrated from the peridotite portion of the slab interacted with the overlying crust portion (i.e. ‘slab rehydration’¹²) before the release to the wedge mantle.

Because δD ‰ values of ~ -60 ‰ at Fukue are representative of the slab fluid beneath the Fukue volcano (Supplementary Method), the δD ‰ values of the residual slab materials that were stored in the MTZ can be estimated to be ~ -90 ‰, assuming the D/H fractionation factor ($1000 \ln \alpha$) between the slab and fluid of -30 ‰ (Ref.⁹ and the references therein). If we consider the possible pressure dependence on the fractionation factor³⁵, the δD ‰ of the residual slab materials could be higher than ~ -90 ‰. Our new estimate of the δD ‰ values for the recycled slab materials is much higher than -234 ‰ estimated by Ref.⁹ and is also slightly higher than -100 ‰ to -120 ‰ obtained by Ref.¹¹. At Koolau volcano (Hawaii) where recycled slab materials are considered to have contributed significantly to the source mantle³⁶, a δD ‰ value of -120 ‰ was estimated¹⁶. If the δD ‰ value of the Earth’s primordial H₂O is -60 to -80 ‰^{13,37}, then the lower δD of -120 ‰ compared to both the primordial δD and the δD ‰ value of > -90 ‰ for slab materials stored in the MTZ may suggest that the recycled materials in the Koolau basalts experienced further D/H fractionation during the transport from the MTZ to the bottom of the mantle as a cold plume and/or during the residence at the core-mantle boundary until the ascent as a hot plume.

Methods

Analytical methods. Whole-rock major and trace element analyses as well as Sr, Nd, and Pb isotopic analyses on the scoria samples were carried out at the Faculty of Science, Hokkaido University, Japan. Major element compositional analyses of melt inclusions and the host olivine crystals were also conducted at Hokkaido University. The details of the analytical methods were provided in Supplementary Methods.

The CO₂, H₂O, F, Cl, S, and P₂O₅ content analyses of the melt inclusions were conducted using an ion microprobe CAMECA IMS-1280HR, AMETEK CAMECA, at the Kochi Institute for Core Sample Research,

JAMSTEC, following the methods described in Ref.²⁰. Melt inclusion-bearing olivine crystals separated from the scoria samples were individually mounted in an acrylic resin, and they were polished until melt inclusions were exposed. The polished crystals were then mounted in an indium-filled Al-disc of 1 inch to minimise volatile background. To dry the sample completely, the cleaned Al-disc was kept in an oven at 80 °C and 10⁻⁷ torr for more than 48 h prior to Au coating. The Au-coated Al-disc was stored in the airlock chamber of the spectrometer at < 10⁻⁸ torr overnight prior to the analyses.

We used a 20 keV Cs⁺ primary beam of 500 pA defocused to a diameter of 10–15 μm. A – 10 keV electron gun of ~ 100 μm in diameter was used to avoid charging the sample surface. We set the field aperture size to 5 × 5 μm of the field of view of the secondary ion image to eliminate secondary ion signals from surface contamination. The instrument was operated with a mass resolving power of ~ 6000, which allows us to distinguish completely the interferences of ³⁴S¹H on ³⁵Cl, ¹⁷O on ¹⁶O¹H, ²⁹Si¹H on ³⁰Si, and ³¹P¹H on ³²S. We detected negative secondary ions of ¹²C, ¹⁶OH, ¹⁹F, ³⁰Si, ³¹P, ³²S, and ³⁵Cl by an axial electron multiplier using a magnetic peak switching method. The total measurement time for each analysis, including 20 s for pre-sputtering, 120 s for auto-centring of secondary ions, and 10 cycles for measurements, was ~ 7 min. Fourteen in-house basaltic glass standards with broad ranges of volatile contents were used²⁰. The concentrations of volatiles and P₂O₅ in melt inclusions were determined by calibration curves of the ³⁰Si-normalised intensities of volatile elements and ³¹P of a set of basaltic standards. Analytical reproducibilities of CO₂, H₂O, F, P₂O₅, S, and Cl concentrations were 3.6, 0.8, 2.0, 0.9, 0.8, and 1.3%, respectively, which were obtained by repeated analyses (n = 72) on different glass fragments (n = 38) of a homogeneous MORB basalt (EPR-G3) over seven analytical sessions. The maximum uncertainties were less than 5% for H₂O, 15% for CO₂, and 10% for Cl, F, S, and P₂O₅.

The hydrogen isotope analyses were conducted on the same melt inclusions as those used for the volatile content analyses. The same microprobe as above was used, and a method described in Ref.²¹ was followed. We used a 20 keV Cs⁺ ion beam of ~ 5 nA defocused to ~ 15 μm in diameter. A – 10 keV electron gun of ~ 100 μm in diameter was used. We set the field aperture size to 7 × 7 μm, which is smaller than the beam size, to minimise hydrogen contamination from the edge of the primary beam. We measured negative secondary ions of ¹⁶OH⁻ and ¹⁶OD⁻ in multi-detection mode with a Faraday cup (FC) of 10⁺¹¹ or 10⁺¹² Ω resistance and axial electron multiplier, respectively. To sufficiently separate the ¹⁶OD⁻ from ¹⁸O⁻, ¹⁷OH⁻, and ¹⁶OHH⁻, we set the mass resolving power (M/ΔM) of the axial detector to approximately 10,000. The mass resolving power of the FC detector was set to ~ 5000 with a slit of 250 μm in width, allowing sufficient separation of the ¹⁶OH⁻ signal from the ¹⁷O⁻ signal. The total measurement time for each analysis, including 20 s pre-sputtering, ~ 120 s for auto-centring of ¹⁶OH⁻ to the field and contrast apertures, and 4 s × 50 cycles for measurements, was ~ 6 min. FC background stability was ~ 700 cps (2sd), which did not affect the D/H ratios as long as OH was > 0.4 Mcps or H₂O was > 0.2 wt.%.

Three in-house basaltic glass standards were used for the calibration of the analyses. The water contents and δD‰ values are 0.54 wt.% and – 107 ± 20‰ (2sd), 0.94 wt.% and – 109 ± 3‰, and 3.6 wt.% and 37 ± 5‰, respectively. The δD‰ values were determined by TCEA/IRMS (high-temperature conversion elemental analyser/isotope ratio mass spectrometer). The standard bracketing method was adopted to determine the D/H ratios of the melt inclusions. The working standard of Hawaiian submarine basaltic glass (H₂O content of 1.4 wt.% and δD‰ of – 95 ± 5‰) was embedded in the sample mount, and it was measured five times for every ten unknown samples. We calculated the instrumental mass fractionation factor and analytical error by averaging 10 data points of the standard glass. If the 2se of the melt inclusion was greater than the 2sd, we adopted the former as the analytical error; otherwise, the latter was adopted as the analytical error. Water contents of the melt inclusions were typically higher than that of the working standard in this study, and hence, analytical errors of most melt inclusions were 2sd of the working standard averages of each bracket.

Data availability

The datasets generated and/or analysed during the current study are available from the corresponding author upon reasonable request.

Received: 14 June 2021; Accepted: 6 September 2021

Published online: 21 September 2021

References

- Walker, J. C. G. *Evolution of the Atmosphere* (Macmillan, 1977).
- McGovern, P. J. & Schubert, G. Thermal evolution of the Earth: Effects of volatile exchange between atmosphere and interior. *Earth Planet. Sci. Lett.* **96**, 27–37 (1989).
- Hirschmann, M. M. Water, melting, and the deep Earth H₂O cycle. *Annu. Rev. Earth Planet. Sci.* **34**, 629–653 (2006).
- Peslier, A. H., Schönbächler, M., Busemann, H. & Karato, S.-I. Water in the Earth's interior: Distribution and origin. *Space Sci. Rev.* **212**, 743–810 (2017).
- Bekaert, D. V. *et al.* Subduction-driven volatile recycling: A global mass balance. *Annu. Rev. Earth Planet. Sci.* **49**, 37–70 (2021).
- Craig, H. & Lupton, J. E. Primordial neon, helium, and hydrogen in oceanic basalts. *Earth Planet. Sci. Lett.* **31**, 369–385 (1976).
- Kyser, T. K. & O'Neil, J. R. Hydrogen isotope systematics of submarine basalts. *Geochim. Cosmochim. Acta* **48**, 2123–2133 (1984).
- Poreda, R., Schilling, J. G. & Craig, H. Helium and hydrogen isotopes in ocean-ridge basalts north and south of Iceland. *Earth Planet. Sci. Lett.* **78**, 1–17 (1986).
- Shaw, A. M., Hauri, E. H., Fischer, T. P., Hilton, D. R. & Kelley, K. A. Hydrogen isotopes in Mariana arc melt inclusions: Implications for subduction dehydration and the deep-Earth water cycle. *Earth Planet. Sci. Lett.* **275**, 138–145 (2008).
- Hallis, L. J. *et al.* Evidence for primordial water in Earth's deep mantle. *Science* **350**, 795–797 (2015).
- Walowski, K. J., Wallace, P. J., Hauri, E. H., Wada, I. & Clynne, M. A. Slab melting beneath the Cascade Arc driven by dehydration of altered oceanic peridotite. *Nat. Geosci.* **8**, 404–408 (2015).
- Dixon, J. E. *et al.* Light stable isotopic compositions of enriched mantle sources: Resolving the dehydration paradox. *Geochem. Geophys. Geosyst.* **18**, 3801–3839 (2017).

13. Loewen, M. W., Graham, D. W., Bindeman, I. N., Lupton, J. E. & Garcia, M. O. Hydrogen isotopes in high $^3\text{He}/^4\text{He}$ submarine basalts: Primordial vs. recycled water and the veil of mantle enrichment. *Earth Planet. Sci. Lett.* **508**, 62–73 (2019).
14. Dixon, J. E., Leist, L., Langmuir, C. & Schilling, J.-G. Recycled dehydrated lithosphere observed in plume-influenced mid-ocean ridge basalt. *Nature* **420**, 385–389 (2002).
15. Syracuse, E. M. & Abers, G. A. Global compilation of variations in slab depth beneath arc volcanoes and implications. *Geochem. Geophys. Geosyst.* **7**, Q05017 (2006).
16. Hauri, E. SIMS analysis of volatiles in silicate glasses, 2: Isotopes and abundances in Hawaiian melt inclusions. *Chem. Geol.* **183**, 115–141 (2002).
17. Bucholz, C. E., Gaetani, G. A., Behn, M. D. & Shimizu, N. Post-entrapment modification of volatiles and oxygen fugacity in olivine-hosted melt inclusions. *Earth Planet. Sci. Lett.* **374**, 145–155 (2013).
18. Kelbert, A., Schultz, A. & Egbert, G. Global electromagnetic induction constraints on transition-zone water content variations. *Nature* **460**, 1003–1006 (2009).
19. Kuritani, T., Sakuyama, T., Kamada, N., Yokoyama, T. & Nakagawa, M. Fluid-fluxed melting of mantle versus decompression melting of hydrous mantle plume as the cause of intraplate magmatism over a stagnant slab: Implications from Fukue Volcano Group, SW Japan. *Lithos* **282–283**, 98–110 (2017).
20. Shimizu, K. *et al.* H_2O , CO_2 , F, S, Cl, and P_2O_5 analyses of silicate glasses using SIMS: Report of volatile standard glasses. *Geochem. J.* **51**, 299–313 (2017).
21. Shimizu, K., Ushikubo, T., Murai, T., Matsu'ura, F. & Ueno, Y. In situ analyses of hydrogen and sulfur isotope ratios in basaltic glass using SIMS. *Geochem. J.* **53**, 195–207 (2019).
22. Newman, S., Epstein, S. & Stolper, E. Water, carbon dioxide, and hydrogen isotopes in glasses from the ca. 1340 A.D. eruption of the Mono Craters, California: Constraints on degassing phenomena and initial volatile content. *J. Volcanol. Geotherm. Res.* **35**, 75–96 (1988).
23. Dixon, J. E. & Stolper, E. M. An experimental study of water and carbon dioxide solubilities in mid-ocean ridge basaltic liquids. Part II: Applications to degassing. *J. Petrol.* **36**, 1633–1646 (1995).
24. Wallace, P. J. Volatiles in subduction zone magmas: Concentrations and fluxes based on melt inclusion and volcanic gas data. *J. Volcanol. Geotherm. Res.* **140**, 217–240 (2005).
25. Rose-Koga, E. F. *et al.* Volatile (F and Cl) concentrations in Iwate olivine-hosted melt inclusions indicating low-temperature subduction. *Earth Planets Space* **66**, 81 (2014).
26. Shimizu, K. *et al.* Identifying volatile mantle trend with the water-fluorine-cerium systematics of basaltic glass. *Chem. Geol.* **522**, 283–294 (2019).
27. Zhao, D., Lei, J. & Tang, R. Origin of the Changbai intraplate volcanism in Northeast China: Evidence from seismic tomography. *Chin. Sci. Bull.* **49**, 1401–1408 (2004).
28. Ohtani, E. & Zhao, D. The role of water in the deep upper mantle and transition zone: Dehydration of stagnant slabs and its effects on the big mantle wedge. *Russ. Geol. Geophys.* **50**, 1073–1078 (2009).
29. Bernini, D., Wiedenbeck, M., Dolejš, D. & Keppler, H. Partitioning of halogens between mantle minerals and aqueous fluids: Implications for the fluid flow regime in subduction zones. *Contrib. Mineral. Petrol.* **165**, 117–128 (2013).
30. Clog, M., Aubaud, C., Cartigny, P. & Dosso, L. The hydrogen isotopic composition and water content of southern Pacific MORB: A reassessment of the D/H ratio of the depleted mantle reservoir. *Earth Planet. Sci. Lett.* **381**, 156–165 (2013).
31. Kimura, J.-I. & Nakajima, J. Behaviour of subducted water and its role in magma genesis in the NE Japan arc: A combined geo-physical and geochemical approach. *Geochim. Cosmochim. Acta* **143**, 165–188 (2014).
32. England, P., Engdahl, R. & Thatcher, W. Systematic variation in the depths of slabs beneath arc volcanoes. *Geophys. J. Int.* **156**, 377–408 (2004).
33. Holt, A. F., Royden, L. H., Becker, T. W. & Faccenna, C. Slab interactions in 3-D subduction settings: The Philippine Sea Plate region. *Earth Planet. Sci. Lett.* **489**, 72–83 (2018).
34. van Keken, P. E., Hacker, B. R., Syracuse, E. M. & Abers, G. A. Subduction factory: 4. Depth-dependent flux of H_2O from subducting slabs worldwide. *J. Geophys. Res.* **116**, B01401 (2011).
35. Horita, J., Driesner, T. & Cole, D. R. Hydrogen isotope fractionation in the system brucite-water \pm NaCl to elevated temperatures and pressures: Implications for the isotopic property of NaCl fluids under geologic conditions. *Geochim. Cosmochim. Acta* **235**, 140–152 (2018).
36. Hauri, E. H. Major-element variability in the Hawaiian mantle plume. *Nature* **382**, 415–419 (1996).
37. Lécuyer, C., Gillet, P. & Robert, F. The hydrogen isotope composition of seawater and the global water cycle. *Chem. Geol.* **145**, 249–261 (1998).
38. Kita, S., Okada, T., Hasegawa, A., Nakajima, J. & Matsuzawa, T. Existence of interplane earthquakes and neutral stress boundary between the upper and lower planes of the double seismic zone beneath Tohoku and Hokkaido, northeastern Japan. *Tectonophysics* **496**, 68–82 (2010).
39. Liu, X. & Zhao, D. Backarc spreading and mantle wedge flow beneath the Japan Sea: Insight from Rayleigh-wave anisotropic tomography. *Geophys. J. Int.* **207**, 357–373 (2016).
40. Liu, J., Han, J. & Fyfe, W. S. Cenozoic episodic volcanism and continental rifting in northeast China and possible link to Japan Sea development as revealed from K-Ar geochronology. *Tectonophysics* **339**, 385–401 (2001).
41. Zhao, D., Yu, S. & Ohtani, E. East Asia: Seismotectonics, magmatism and mantle dynamics. *J. Asian Earth Sci.* **40**, 689–709 (2011).
42. Kimura, J.-I. Modeling chemical geodynamics of subduction zones using the Arc Basalt Simulator version 5. *Geosphere* **13**, 992–1025 (2017).
43. Kuritani, T. *et al.* Primary melt from Sannome-gata volcano, NE Japan arc: Constraints on generation conditions of rear-arc magmas. *Contrib. Mineral. Petrol.* **167**, 969 (2014).
44. Kuritani, T., Kanai, C., Yamashita, S. & Nakagawa, M. Magma generation conditions at the Akita-Komagatake volcano, Northeast Japan arc: Implications of across-arc variations in mantle melting parameters. *Lithos* **348–349**, 105197 (2019).

Acknowledgements

We thank Dr. Akiko Matsumoto for helping with the electron probe micro-analyser and X-ray fluorescence analyses. Fruitful comments by Prof. Jackie Dixon and two anonymous reviewers substantially improved the manuscript. We also thank Prof. Christoph Beier for editorial handling. This study was supported by research grants from the Japan Society for the Promotion of Science KAKENHI (Grant Numbers 16K13900 and 25287144 to T.K. and 18H01320 to K.S.) and the Ministry of Education, Culture, Sports, Science and Technology (MEXT) of Japan under its Earthquake and Volcano Hazards Observation and Research Program and the Integrated Program for Next Generation Volcano Research and Human Resource Development.

Author contributions

T.K. and K.S. conceived this study. T.K., M.N., H.T., E.S., and N.D. collected the rock samples, and T.K., K.S., and T.U. conducted the analyses. T.K., K.S., T.U., Q.-K.X., J.L., and M.N. contributed to the interpretation of the data. T.K. led the manuscript preparation efforts with input from K.S., T.U., Q.-K.X., J.L., and M.N.

Competing interests

The authors declare no competing interests.

Additional information

Supplementary Information The online version contains supplementary material available at <https://doi.org/10.1038/s41598-021-98307-y>.

Correspondence and requests for materials should be addressed to T.K.

Reprints and permissions information is available at www.nature.com/reprints.

Publisher's note Springer Nature remains neutral with regard to jurisdictional claims in published maps and institutional affiliations.



Open Access This article is licensed under a Creative Commons Attribution 4.0 International License, which permits use, sharing, adaptation, distribution and reproduction in any medium or format, as long as you give appropriate credit to the original author(s) and the source, provide a link to the Creative Commons licence, and indicate if changes were made. The images or other third party material in this article are included in the article's Creative Commons licence, unless indicated otherwise in a credit line to the material. If material is not included in the article's Creative Commons licence and your intended use is not permitted by statutory regulation or exceeds the permitted use, you will need to obtain permission directly from the copyright holder. To view a copy of this licence, visit <http://creativecommons.org/licenses/by/4.0/>.

© The Author(s) 2021